Title
Bone Biomarkers Based on Magnetic Resonance Imaging

Journal
Seminars in Musculoskeletal Radiology, 28(01)

ISSN
1098-898X

Authors
Jerban, Saeed
Jang, Hyungseok
Chang, Eric Y
et al.

Publication Date
2024-02-01

DOI
10.1055/s-0043-1776431

Peer reviewed

Article published online: 2024-02-08

Bone Biomarkers Based on Magnetic Resonance Imaging

Saeed Jerban, PhD[1] Hyungseok Jang, PhD[1] Eric Y. Chang, MD[1,2] Susan Bukata, MD[3] Jiang Du, PhD[1,2,4] Christine B. Chung, MD[1,2]

[1] Department of Radiology, University of California, San Diego, La Jolla, California
[2] Research Service, Veterans Affairs San Diego Healthcare System, San Diego, California
[3] Department of Orthopaedic Surgery, University of California, San Diego, La Jolla, California
[4] Department of Bioengineering, University of California, San Diego, La Jolla, California

Address for correspondence Saeed Jerban, PhD, Department of Radiology, University of California, San Diego, 9500 Gilman Drive, La Jolla, CA 92093 (e-mail: sjerban@health.ucsd.edu).

Semin Musculoskelet Radiol 2024;28:62–77.

Abstract

Magnetic resonance imaging (MRI) is increasingly used to evaluate the microstructural and compositional properties of bone. MRI-based biomarkers can characterize all major compartments of bone: organic, water, fat, and mineral components. However, with a short apparent spin-spin relaxation time (T2*), bone is invisible to conventional MRI sequences that use long echo times. To address this shortcoming, ultrashort echo time MRI sequences have been developed to provide direct imaging of bone and establish a set of MRI-based biomarkers sensitive to the structural and compositional changes of bone. This review article describes the MRI-based bone biomarkers representing total water, pore water, bound water, fat fraction, macromolecular fraction in the organic matrix, and surrogates for mineral density. MRI-based morphological bone imaging techniques are also briefly described.

Keywords
- magnetic resonance imaging
- cortical bone
- trabecular bone
- biomarkers
- ultrashort echo time

Bone structures can be classified as cortical bone (compact bone) or trabecular bone (spongy bone).[1] Bone ultrastructural elements are composed of mineral matrix (40–70% by volume), organic matrix (20–40%), water (10–30%), and fat (< 5%).[1–3] Bone mineral provides stiffness and strength, particularly during compressive loading; collagen provides ductility and the ability to absorb energy before fracture. Bone contains more water at trabecular sites, in combination with fat in bone marrow that typically occupies > 80% of the bone volume. Water and fat combined in trabecular bone sites may increase up to 95% of the total volume in patients with osteoporosis (OPo).[4,5] In addition to the water present in marrow, a fraction of bone water called pore water (PW) resides in pores of various sizes in cortical and trabecular bone elements, including Haversian canals (10–200 µm), lacunae (1–10 µm), and canaliculi (0.1–1 µm).[1,2,6] Most of the bone water in cortical bone is called bound water (BW) that is bound to the organic and mineral matrixes.[6–12]

Bone formation and resorption, also called bone remodeling, occur continuously to replace the old bone regions with new bone structures to respond to supposedly systemic and mechanical skeletal needs.[1,13,14] Clinical biomarkers of bone remodeling have been used in several investigations focused on bone fracture prediction, bone healing, aging, OPo progression, and clinical interventions.[1,15–18] Clinical bone formation biomarkers are products of osteoblastic activity, forming new bone structures. Three main groups of bone formation biomarkers are (1) by-products of collagen type I synthesis (e.g., propeptide of type I collagen such as C-terminal: P1CP and N-terminal: P1NP); (2) osteoblast enzymes such as alkaline phosphatase (enzyme present in the plasma membrane of the osteoblasts); and (3) bone matrix proteins synthesized by osteoblasts such as

Issue Theme Biomarkers; Guest Editor, Richard Kijowski, MD

Thieme Medical Publishers, Inc., 333 Seventh Avenue, 18th Floor, New York, NY 10001, USA

DOI https://doi.org/10.1055/s-0043-1776431.
ISSN 1089-7860.

osteocalcin, a hydroxyapatite-binding protein (i.e., GLA protein constituting 15% of the noncollagenous bone matrix).[18]

In contrast, clinical bone resorption biomarkers are products of active osteoclastic activity, resorbing the old bone structure. Four main groups of bone resorption biomarkers are (1) collagen degradation products, such as telopeptides of type I collagen (e.g., CTX-1), hydroxyproline, and pyridinium crosslinks (e.g., pyridinoline [PYD]); (2) noncollagenous proteins (e.g., sialoprotein); (3) osteoclastic enzymes (e.g., tartrate-resistant acid phosphatase and cathepsin K); and (4) osteocyte activity markers (e.g., receptor activator of nuclear factor κ-B ligand).[18] Monitoring at least one marker of bone formation (e.g., serum P1NP) and a marker of bone resorption (e.g., serum CTX) has been recommended as reference markers in bone-related observational and intervention studies.[17,18] However, bone structure and composition may undergo largely different rates of changes locally versus systemically; the latter can be detected by clinical biomarkers.

The development of noninvasive imaging techniques to characterize bone structural status is of great interest to the orthopaedic and radiology communities. The World Health Organization defined OPo based on the areal bone mineral density (aBMD) measured locally at the hip or spine using the dual-energy X-ray absorptiometry (DEXA) imaging modality.[19] Specifically, patients with an aBMD ≤ 2.5 standard deviations than the average aBMD of the young population (T-score ≤ -2.5) are diagnosed with OPo. Osteopenia (OPe) is a condition that precedes OPo in which the patient's T-score < -1.[20]

Radiograph-based medical imaging biomarkers such as in DEXA, computed tomography (CT), quantitative computed tomography (QCT), and high-resolution peripheral QCT (HR-pQCT) are established based on measuring aBMD or volumetric bone mineral density (vBMD) and rending the spatial distribution of the mineral component of the bone. However, the organic matrix, water, and fat, which together represent between 55% and ~80% of cortical and trabecular bone by volume, respectively, are largely missed in radiograph-based medical imaging biomarkers.[21–24] Moreover, the three-dimensional (3D) radiograph-based medical imaging biomarkers obtained using CT, QCT, and HR-pQCT require exposing the patients to some levels of ionizing radiation that may be concerning in longitudinal investigations. It is noteworthy that newly developed photon-counting detector CT scanners awaiting more validation are significantly limiting ionizing radiation while acquiring relatively high-resolution images.[25]

Ultrasonography (US)-based medical imaging biomarkers have also been developed to assess bone structures, motivated by the need to provide portable, easily accessible, and affordable techniques.[26,27] Such biomarkers have mainly focused on estimating the US wave velocity (or speed of sound), US attenuation, and US backscatter.[28] However, applications of these biomarkers have been mainly limited to the superficial sites of the skeleton,[27,29–38] likely due to the artifacts associated with US modality assessing deep body sites, bone's high US impedance, operator dependencies, and the absence of validated US tomography attuned for bone tissue.

Magnetic resonance imaging (MRI) has been increasingly used to evaluate the nonmineral portions of bone.[39–41] Remarkably, MRI-based bone evaluation can also provide valuable assessment of the surrounding soft tissues, such as ligaments, tendons, and muscles, which is an advantage not achievable with radiograph-based biomarkers. However, bone is invisible to conventional MRI sequences currently used in clinics.[42]

Specifically, the bone structure has a short apparent transverse relaxation time ($T2^* < 0.5$ ms); therefore, typical conventional clinical MRI pulse sequences with echo times (TEs) of a few milliseconds cannot capture the returned radiofrequency (RF) signal from bone.[43,44] To address this shortcoming, ultrashort echo time (UTE) MRI sequences have been developed to provide direct imaging of bone and establish a set of MRI-based biomarkers sensitive to bone structural and compositional changes.[12,45–47] The basic 3D UTE sequence uses a short RF rectangular pulse for signal excitation followed by 3D radial ramp sampling with minimal nominal TEs of 0.008 to 0.050 ms, depending on the hardware. Such a quick MR signal acquisition allows UTE MRI to detect total water (TW), including both BW and PW components, of the bone structures.[10] Several pulse sequence preparations, signal acquisition, and modeling techniques combined with UTE MRI have been proposed in the literature to characterize all other major components of the bone.

This review article summarizes the reported MRI-based bone biomarkers representing different bone components, such as TW, PW, BW, fat fraction (FF), macromolecules in the organic matrix, and surrogates of mineral density in the cortical bone. MRI-based morphological bone imaging techniques are also briefly described.

MRI-based Bone Morphological Imaging

Conventional MRI sequences generally visualize the bone tissue with a signal void surrounded by a bright signal from adjacent soft tissues, such as muscle, skin, and bone marrow. Such an indirect visualization of bone elements has been used for morphological imaging of cortical and trabecular bone; the latter requires high-resolution acquisitions. Image postprocessing enables extracting the 3D architecture and morphological parameters of cortical and trabecular bone.[48–52] Gradient-echo (GRE) and spin-echo (SE) clinical acquisitions have been used for high-resolution trabecular bone imaging.[53] GRE-based techniques result in a shorter scanning process due to shorter achievable repetition times (TRs).[53] SE-based techniques lead to less distortion of signal intensity in the bone structure and more realistic trabecular sizes.[53] Considering the average size of trabeculae, the in-plane MRI pixel sizes are often selected to be < 0.2 mm when spongy bone regions are focused. ►**Fig. 1a** shows indirect morphological imaging of the tibial and fibular shafts using a conventional GRE sequence. ►**Fig. 1b** demonstrates indirectly visualized trabeculae in bright bone marrow performed with a steady-state free precession spin-echo sequence.[53]

In addition to the indirect morphological imaging of bone, several MRI sequences are capable of direct bone morphological imaging. PW may constitute up to a quarter of the bone elements' volume and possesses a short $T2^*$ but a

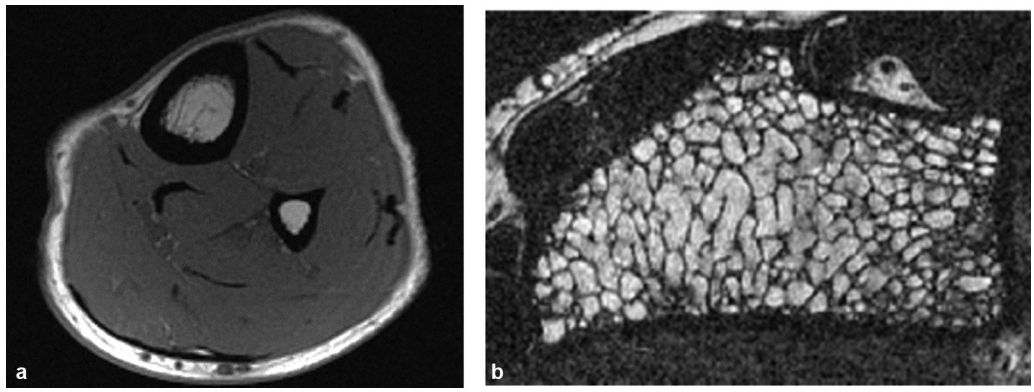

Fig. 1 Indirect visualization of (**a**) cortical bone in tibial and fibular shafts using conventional gradient-echo sequence and (**b**) trabecular bone in distal tibial metaphysis using the steady-state free precession spin-echo sequence. Note: Image in (b) was previously presented by Techawiboonwong et al.[142] The reprinting permission is granted through the RightsLink system. The figure is modified for presentation purposes. Minor modifications were made for presentation purposes.

relatively long T2 (up to 100 ms).[7,8,10,54] Therefore, some conventional fast spin-echo (FSE)[55] and short echo-time sequences have the potential to image PW in bone that accumulates more in highly porous cortical bone sites (e.g., near endosteum). Direct morphological imaging of cortical bone with low porosity requires more advanced MRI techniques, such as UTE, adiabatic inversion recovery UTE (IR-UTE), dual-inversion recovery UTE (dual-IR-UTE), double-inversion recovery UTE (double-IR-UTE), UTE with rescaled echo subtraction (UTE-RS), fat-suppressed UTE, water- and fat-suppressed proton projection imaging (WASPI), spectral presaturation with inversion recovery (SPIR), and zero echo time (ZTE) sequences.[12,40] ►**Fig. 2** shows conventional SE, basic UTE, and IR-UTE imaging of the femoral midshaft in a healthy 41-year-old woman. Bone demonstrates zero signal and negative contrast in the clinical sequence, high signal and negative contrast in the UTE MRI sequence, and high signal and positive contrast in the IR-UTE sequence.

Direct morphological imaging of trabecular bone needs long-T2 signal (particularly from the marrow fat) suppression, achievable using IR-UTE, dual-IR-UTE, double-IR-UTE, WASPI, and SPIR sequences. It should be noted that MRI sequences are sensitive to chemical shift artifacts that manifest as spatial blurring and ringing artifacts in non-Cartesian sampling, particularly in the trabecular bone region.[56] The chemical shift artifacts from fat often are much stronger than bone signal in UTE MRI because fatty marrow has a much higher signal than trabecular bone elements. Therefore, no high-resolution direct trabecular bone imaging has been reported so far in the literature to our knowledge.

►**Table 1** briefly compares the MRI techniques just mentioned for direct morphological bone imaging. More details of bone morphological imaging are provided in previous review articles.[12,40]

Water Content Biomarkers

►**Table 2** summarizes the reviewed MRI-based bone biomarkers representing different bone components. UTE MRI has been used in several studies to estimate the water content biomarkers in the cortical bone. Water contents, described as TW, BW, or PW, are key components in MRI bone biomarkers, described in the following sections.

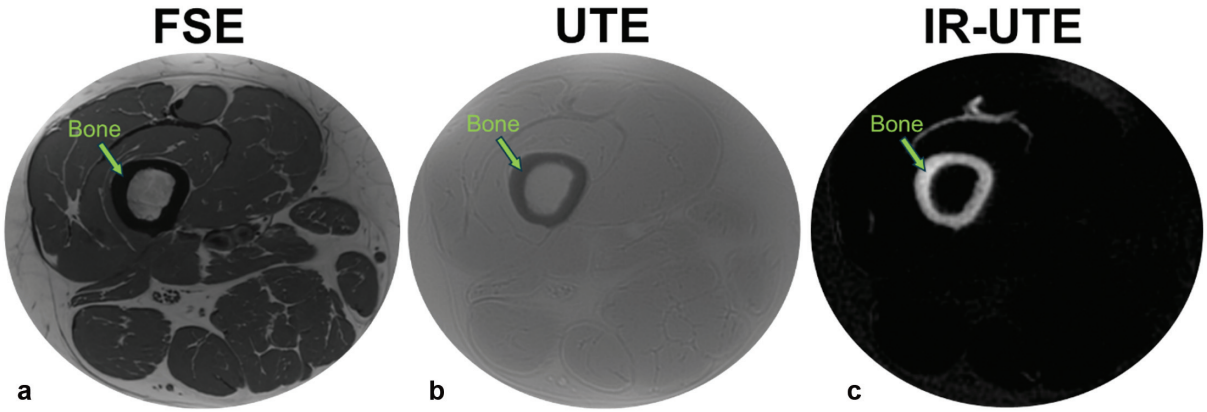

Fig. 2 Representative axial images of the femoral midshaft of a healthy 41-year-old woman using (**a**) a clinical fast spin-echo sequence, (**b**) an ultrashort echo time (UTE)-Cones sequence, and (**c**) an inversion recovery (IR)-UTE sequence. Bone demonstrates zero signal and negative contrast in the clinical sequence, high signal and negative contrast in the UTE MRI sequence, and high signal and positive contrast in the IR-UTE sequence.

Table 1 Comparison of direct morphological bone magnetic resonance imaging techniques

MRI technique	Relative bone signal	Visualized proton pool	Contrast	Cortical or trabecular bone	Scan time
Conventional FSE[55]	Very low	Water in large pores	High (reverse contrast)	Partial cortical bone	Short
Conventional STE[120]	Very low	Water in large pores	High (reverse contrast)	Partial cortical bone	Short
Basic UTE[6–9,12]	High	Bound and pore water	Low	Cortical bone	Relatively short
UTE-RS[121,122]	High	Bound and pore water	High	Cortical bone	Moderate
ZTE[123–127]	Moderate (low flip angle)	Bound and pore water	Low	Cortical bone	Relatively short
IR-UTE[43,57,58,64,68,76,85,86,128–130]	High	Bound water	High	Cortical and trabecular bone	Long
Dual-IR UTE[68,131,132]	High	Bound water	High	Cortical and trabecular bone	Long
Double-IR UTE[133]	High	Bound water	High	Cortical and trabecular bone	Long
Fat-suppression UTE[75,88,89]	High	Bound and pore water	Moderate	Cortical and trabecular bone	Moderate
WASPI[134–137]	High	Bound water	High	Cortical and trabecular bone	Relatively long
SPIR[75]	High	Bound water	High	Cortical and trabecular bone	Relatively long

Abbreviations: FSE, fast spin echo; IR, inversion recovery; SPIR, spectral presaturation with inversion recovery; STE, short echo time; UTE, ultrashort echo time; WASPI, water- and fat-suppressed proton projection imaging; ZTE, zero echo time.

Table 2 Comparison of the quantitative bone magnetic resonance imaging biomarkers

	UTE MRI technique	Biomarker	Scan time	Predicted bone characteristics
Cortical bone	Basic UTE (plus phantom imaging)[57–62,64–66,102,138]	TW density	Short	- Correlated positively with cortical bone porosity and negatively with vBMD (μCT)[64,65] - Higher TW was associated with OPo[66] - Correlated negatively with aBMD (DEXA) and vBMD (HR-pQCT)[66]
	IR-UTE (plus phantom imaging)[57,58,62,64,66,71]	BW density	Moderate	- Correlated positively with cortical bone stiffness, strength, and toughness to fracture[69,72]
	DAEF-UTE (plus phantom imaging)[57,69]	PW density	Moderate	- Correlated positively with bone porosity (μCT) and negatively with stiffness, strength, and toughness to fracture[69,72]
	IR-UTE and UTE subtraction (plus phantom imaging)[59,64,66,73]	PW density	Moderate	- Correlated positively with cortical bone porosity and negatively with vBMD (μCT)[64] - Higher PW was associated with OPo[66] - Correlated negatively with aBMD (DEXA) and vBMD (HR-pQCT)[66]
	Bicomponent UTE fitting[10,81,83,84,139]	BW and PW relative contents and T2*s	Long	- PW and BW fractions were correlated with cortical bone porosity (μCT and

(*Continued*)

Table 2 (*Continued*)

	UTE MRI technique	Biomarker	Scan time	Predicted bone characteristics
				histomorphometry) and vBMD, stiffness, and strength.[81,83,84,91] PW and BW correlations were inverse
	Tricomponent UTE fitting[90,91]	BW, PW, and fat relative contents and T2*s	Long	- PW and BW fractions were correlated with cortical bone porosity (μCT) and vBMD, stiffness, and strength.[90,91] PW and BW correlations were inverse
	UTE to IR-UTE signal fraction[60,77,78]	TW-to-BW ratio (SR)	Moderate	- SR was correlated positively with cortical bone porosity (μCT), age,[60,78] aBMD (DEXA), and vBMD (HR-pQCT)[66,77] - Higher SR was associated with OPo and OPe[66,77]
	Dual TE signal fraction[77–80]	PW-to-TW ratio (PI)	Short	- Correlated positively with cortical bone porosity (μCT), vBMD, and donor age and negatively with mechanical stiffness and collagen estimation from near-infrared spectroscopy.[78–80] - Higher PI was associated with OPo[66,77]
	Basic UTE signal decomposition model[74]	BW-to-PW ratio	Short	- PW fraction was correlated positively with subject age[74] The correlations of the BW fraction were inverse
	UTE-MT modeling[64,82,83,92–95,140,141]	Macromolecular proton-to-total proton ratio (MMF)	Long	- MMF was correlated negatively with cortical bone porosity (μCT and histomorphometry) and positively with vBMD, stiffness, and strength[64,82,83,92–95,140,141]
	UTE-MT modeling and basic UTE (plus phantom imaging)[64]	MMPD	Long	- Correlated negatively with cortical bone porosity (μCT) and subject age[64]
	UTE QSM[96,97]	Magnetic susceptibility (BMD estimation)	Long	- Correlated negatively with cortical bone porosity (μCT) and positively with vBMD[97]
	Basic UTE or ZTE at ^{31}P frequency[44,58,60,62,102]	Phosphorous content (BMD estimation)	Moderate	- UTE feasibility studies were performed[44,58] - Lower 31P was associated with aging and OPo[102]
Trabecular bone	SPIR UTE[75]	BW T2*	Moderate	- Correlated positively with cortical bone porosity (μCT)[75]
	IR-UTE[76]	BW density and T2*	Moderate	- Feasibility studies were performed[76]

Abbreviations: aBMD, areal bone mineral density; BMD, bone mineral density; BW, bound water; DEXA, dual-energy X-ray absorptiometry; HR-pQCT, high-resolution peripheral quantitative computed tomography; IR, inversion recovery; MMF, macromolecular proton fraction; MMPD, macromolecular proton density; MT, magnetization transfer; OPe, osteopenia; OPo, osteoporosis; PI, porosity index; PW, pore water; QSM, quantitative susceptibility map; SPIR, spectral presaturation with inversion recovery; SR, suppression ratio; TW, total water; μCT, micro computed tomography; UTE, ultrashort echo time; vBMD, volumetric bone mineral density; ZTE, zero echo time.

Total Water Biomarker Using Basic Ultrashort Echo Time

The TW content of cortical bone can be estimated by comparing the UTE MRI signal of bone with that of an external reference of known proton density (PD).[57–63] The estimated content should be corrected for differences between the T2* and longitudinal relaxation time (T1) values of bone and the external reference.[64] A mixture of distilled water and deuterated water (e.g., 20% H_2O and 80% D_2O, 22 mol/L ^{1}H) with a matched effective T2* of cortical bone (e.g., T2* ≈ 0.4 ms) has been the most common external reference standard in the literature for this

estimation.[57–59,61,64] However, rubber erasers have also been mentioned as external phantoms in this technique because their apparent PD and MRI properties are similar to bone.[65] TW biomarker in cortical bone was shown to be correlated positively with cortical bone porosity and pore size while negatively correlated with vBMD (micro computed tomography [μCT]).[64,65] Moreover, in an in vivo investigation, a higher TW was associated with OPo, and significant negative correlations were observed between TW and BMD (aBMD from DEXA and vBMD from HR-pQCT).[66]

For accurate estimation of TW content, it is recommended to consider, first, the difference between relaxation times of cortical bone and the external standard; second, the spatial variation of the coil sensitivity within the scanned field of view; and third, the duration of the RF pulse and its homogeneity (or actual flip angle [FA]).[59,67] Due to the short T_1 in cortical bone, its effect on the TW content calculation can be neglected if a relatively low FA is used combined with a relatively long TR to produce a PD-weighted UTE sequence.[65]

Bound Water Biomarker Using Inversion Recovery Ultrashort Echo Time

IR-UTE sequences can suppress the long-T2 signal, potentially from PW and fat, and then image BW in bone.[68–70] Comparing the IR-UTE signal from bone with an external reference standard can estimate BW content.[57,58,62,64,71] BW content quantification based on the IR-UTE sequence requires efficient nulling of the PW signal.[59] Bound water proton density (BWPD) demonstrated significant positive correlations with cortical bone stiffness, strength, and toughness to fracture in previous ex vivo investigations.[69,72]

Pore water proton density (PWPD) in the cortical bone can be calculated by subtracting the IR-UTE-measured BWPD from the UTE-measured total water proton density (TWPD).[59,64,66,73] PWPD has shown a significant positive correlation with bone porosity[64] and significant negative correlations with aBMD and vBMD.[64,66] PWPD has also demonstrated lower values in postmenopausal OPo female patients compared with postmenopausal healthy women.[66]

►**Fig. 3** shows in vivo TWPD, BWPD, and PWPD maps in the tibial midshaft of a representative subject with normal bone compared with an OPo patient. The measured tibial TWPD and PWPD were higher, whereas BWPD was lower in the OPo patient than the normal bone subject.

Abbasi-Rad and Saligheh[74] used dual-TR UTE images in the presence of an external reference with known PD to estimate BWPD and PWPD in cortical bone and their corresponding T_1s using a model-based UTE signal decomposition. PWPD and its T_1 demonstrated significant positive correlations with subject age.[74]

Wurnig et al[75] used the SPIR-UTE sequence to measure $T2^*$ of BW in trabecular bone regions after suppressing the long T2 signal at different magnetic field strengths. The bone $T2^*$ values showed significant correlations with bone microstructural parameters obtained from μCT.[75] However, the relatively long $T2^*$ of $\sim$ 2.42 ms for trabecular bone regions at 3 T measured with SPIR-UTE was significantly longer than the

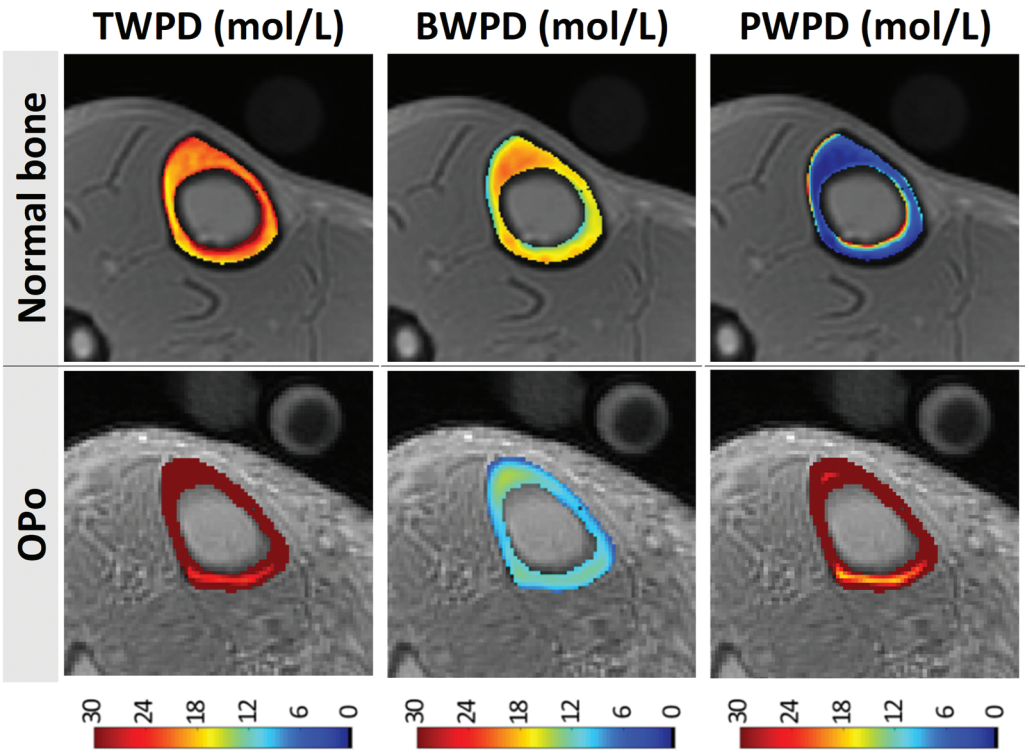

Fig. 3 Generated total water proton-density (TWPD), bound water proton-density (BWPD), and pore water proton-density (PWPD) maps for (first row) a representative subject with normal bone (a 35-year-old woman) and (second row) a representative patient with osteoporosis (OPo) (a 76-year-old woman). For these two examples, tibial TWPD and PWPD were higher; BWPD was lower for the OPo patient compared with the normal bone subject.

T2* of ~ 0.3 ms for cortical bone measured with IR-UTE at the same field strength. This finding was likely due to an incomplete long-T2 signal suppression.

Ma et al[76] used a broadband IR pulse to measure BWPD in trabecular bone and measure BW T2*.[76] A short TR-to-inversion time (TI) ratio was used to improve signal suppression from long-T2 tissues such as muscle and marrow fat. The suppression was followed by multi-spoke UTE acquisition to detect signals from short-T2 water components in trabecular bone. This technique has low sensitivity to B_1 and B_0 inhomogeneities because it uses broadband adiabatic inversion pulses.[76] The technique has been applied ex vivo and in vivo at 3 T and resulted in T2* values (0.3–0.45 ms) comparable with cortical bone measures. BWPD mapping was achieved for trabecular bone by comparing the IR-UTE signals of bone with an external reference.[76] ►**Fig. 4a, b** shows the sagittal lumbar spine images using T2-weighted FSE and IR-UTE sequences, respectively, in a healthy volunteer. ►**Fig. 4c** illustrates the BWPD generated from the IR-UTE images.

Pore Water Biomarker Using Double Adiabatic Full Passage Pulse Ultrashort Echo Time

In addition to the PW calculation by subtracting the IR-UTE-measured BW content from UTE-measured TW content, a double adiabatic full passage pulse was proposed to directly image PW in cortical bone using a pulse preparation to saturate the BW signal followed by a UTE acquisition.[57,69] This technique requires excellent nulling of the BW signal, which can be challenging. Horch et al[69] used UTE MRI at 4.7 T for direct imaging of both BW and PW and reported significant correlations with the mechanical properties of cortical bone strips. Later, Manhard et al[72] used a similar approach and demonstrated a significant correlation between BW measured at 3 T and the bone fracture toughness of cortical bone specimens.

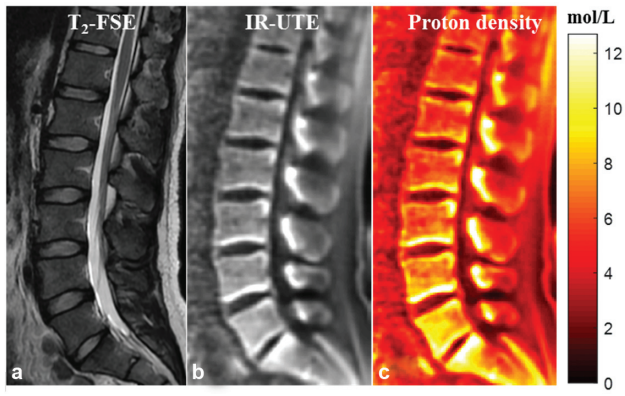

Fig. 4 In vivo qualitative and quantitative imaging of the spine of a 31-year-old male volunteer using the three-dimensional (3D) inversion recovery ultrashort echo time (IR-UTE)-Cones sequence. (**a**) The long T2 muscle and fat are bright in the clinical T2 fast spin-echo image. (**b**) The 3D IR-UTE-Cones image after coil sensitivity correction. (**c**) Proton-density map of the spine trabecular bone. Note: This figure was previously presented by Ma et al.[76] The reprinting permission is granted through the RightsLink system. The figure was modified for presentation purposes. Minor modifications were made for presentation purposes.

Pore Water-to-Total Water Ratio Biomarker Using Dual-echo Ultrashort Echo Time

The signal ratio calculation in dual-echo UTE imaging[77–79] is a rapid UTE-based bone evaluation technique that can be performed in a short time, like the previously mentioned TWPD, BWPD, and PWPD measures (e.g., ~ 5 minutes, depending on the UTE acquisition techniques). This method was proposed by Rajapakse et al[79] to calculate the porosity index (PI), equal to the signal ratio between two MRI images, one with UTE (TE < 0.05 ms) and one with a TE of 2.2 ms. The first echo image represents the total detectable signal from BW, PW, and fat. The second echo represents mostly PW and fat signals that are in-phase at 3 T. BW signal has decayed to near zero at the second echo. Although this technique does not estimate the absolute PWPD or fat content, it can provide an estimation of bone porosity. PI was shown to be positively correlated with cortical bone porosity (μCT), vBMD, and donor age and negatively correlated with mechanical stiffness and collagen estimation from near-infrared spectroscopy.[78–80] Moreover, significantly higher PI was observed in OPo patients compared with OPe and subjects with normal bone.[66,77]

Total Water-to-Bound Water Ratio Biomarker Using Ultrashort Echo Time and Inversion Recovery Ultrashort Echo Time

The signal ratio calculation between UTE and IR-UTE[60] is another example of a relatively rapid UTE-based bone evaluation technique, called the suppression ratio (SR). SR can be performed using dual-band saturation-prepared UTE (DB-UTE) or IR-UTE, aiming to suppress the long-T2 signal before UTE acquisition. SR is a rough estimation of the TW-to-BW ratio and demonstrated significant positive correlations with cortical bone porosity (μCT), age,[60,78] aBMD (DEXA), and vBMD (HR-pQCT) in previous investigations.[66,77] Moreover, significantly higher SR values were reported in OPo patients compared with postmenopausal normal and OPe subjects.[66,77] It should be noted that SR magnitude is sensitive to the selection of TR and TI, and an optimal combination is yet to be investigated for the highest bone evaluation performance.

►**Fig. 5** demonstrates the generated PI and SR pixel maps for three representative female subjects with normal bone, OPe, and OPo conditions.[77] PI and SR values were observed in the following ascending order: normal < OPe < OPo. In contrast, the mean bone thickness was found in the following descending order: normal > OPe > OPo.[77]

Bound Water and Pore Water Biomarkers Using Bicomponent Ultrashort Echo Time Magnetic Resonance Imaging Modeling

The T2* of PW is ~ 10 times the T2* of BW. Thus the BW and PW contributions to the bone signal can be distinguished using UTE MRI acquisition techniques combined with multicomponent T2* analysis.[54,81,82] Such techniques do not estimate absolute water proton content. Multicomponent T2* fitting requires a series of MRI images with different TEs that can extend the scanning process and limit the in vivo applications. Bicomponent exponential T2* fitting was used in many studies to quantify BW and PW biomarkers.[10,81,83] Bae et al[81] and

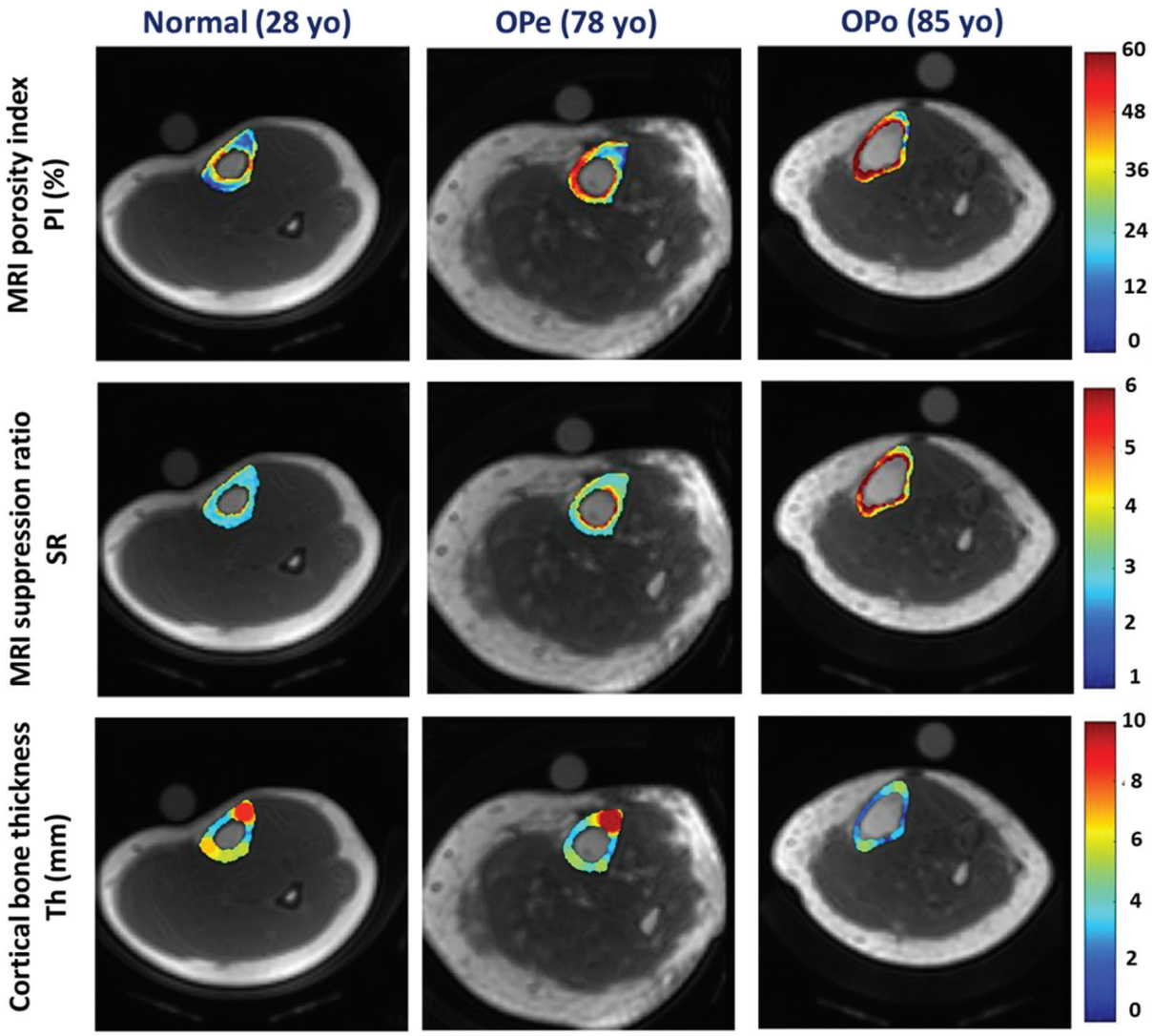

Fig. 5 Generated porosity index (PI), suppression ratio (SR), and bone thickness maps for exemplary subjects from the Normal group (first column, 28-year-old [yo] woman), the osteopenia (OPe) group (second column, 78-yo woman), and the osteoporosis (OPo) group (third column, 85-yo woman). PI and SR were observed in the following ascending order: Normal < OPe < OPo. Regions with higher PI and SR values are likely regions with higher porosity, particularly near the endosteum. In contrast, the mean bone thickness was found in the following descending order: Normal > OPe > OPo. The local bone thickness at each pixel equals the diameter of the largest covering circle. This figure was previously presented by Jerban et al.[77] Reprinting permission is granted under Creative Commons CC-BY license (CC-BY 4.0). The figure is modified for presentation purposes.

Seifert et al[84] found that BW and PW fractions obtained from bicomponent T2* analysis were significantly correlated with µCT-based cortical bone porosity. Bae et al also reported significant correlations between bicomponent T2* results and bone mechanical properties.[81] Jerban et al[83] investigated the efficacy of UTE MRI bicomponent T2* biomarkers in detecting micropores as measured with histomorphometric analysis.[83] Bicomponent T2* was capable of detecting bone porosities, including pores below the range rigorously detectable by µCT.

►**Fig. 6** shows the UTE MRI, µCT, and histology images of a representative anterior tibial bone specimen (of a 71-year-old man).[83] Bone layers closer to the endosteum demonstrate higher porosity and larger pore size. Bicomponent T2* fittings and the histomorphometry pore size distributions within the three bone layers are depicted in the second and third rows of subfigures. The short-T2 fraction (Frac1) was found to be higher in regions with lower porosity and pore size. and peaks in pore size distributions shifted toward lower values for layers closer to the periosteum.[83]

Bound Water, Pore Water, and Fat Fraction Biomarkers Using Tricomponent Ultrashort Echo Time Magnetic Resonance Imaging Modeling

Human cortical bone contains considerable fat, particularly in regions neighboring bone marrow. Different studies have observed oscillation of average MRI signal in multiecho acquisitions with differing TEs used in T2 fitting analyses,[16,85,86] a phenomenon likely caused by fat chemical shift.[87] To remove or separate the fat signal from the bone water signal, fat-suppression techniques such as chemical shift fat saturation (fat-sat), soft-hard water excitation, and

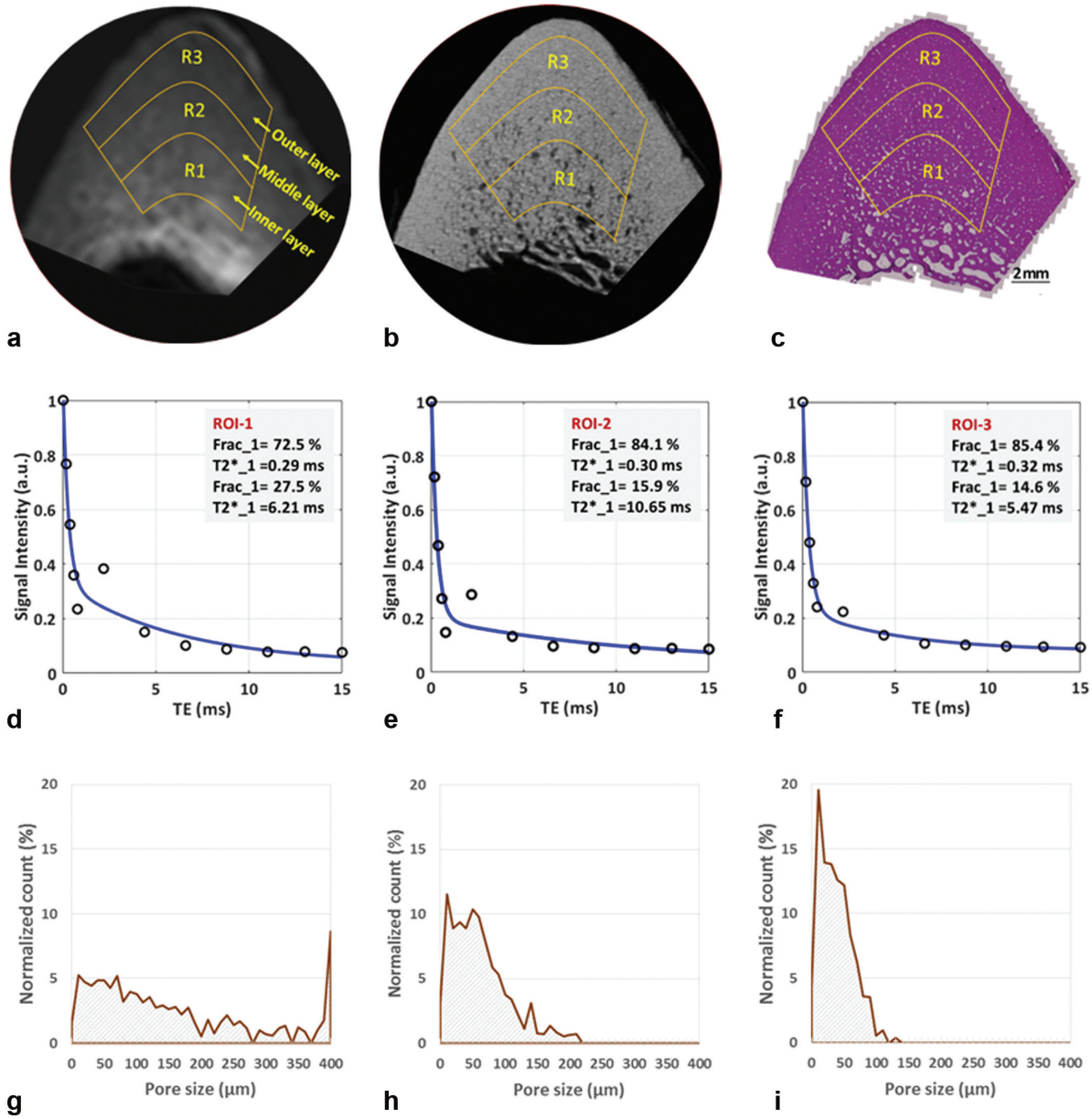

Fig. 6 Analyses based on magnetic resonance imaging (MRI) and histomorphometry for three representative regions of interest (ROIs) in three cortical bone layers. Selected ROIs in three different bone layers on a representative bone specimen (male, 71-year-old) illustrated on (**a**) ultrashort echo time (UTE) MRI (TE = 32 µs; 250 µm pixel size), (**b**) micro computed tomography (µCT) (9 µm pixel size), and (**c**) histology (hematoxylin and eosin stained; 0.2 µm pixel size) images. Bicomponent exponential fitting of the T2* decay within (**d**) region of interest (ROI)-1, (**e**) ROI-2, and (**f**) ROI-3. The oscillating data points indicate the presence of fat, particularly in ROI-1 and ROI-2 near the endosteum. Pore size distribution obtained from histomorphometric analyses are shown for (**g**) ROI-1, (**h**) ROI-2, and (**i**) ROI-3. a.u., arbitrary unit. This figure was previously presented by Jerban et al.[83] Reprinting permission is granted through the RightsLink system. The figure is modified for presentation purposes.

Dixon methods have been used.[88,89] Fat-sat is widely used in clinical MRI sequences; however, it is not suitable for bone imaging due to the saturation of the broad spectrum of bone. A soft-hard pulse was proposed to overcome this effect that uses a low-power soft pulse for fat saturation in the opposite direction of a following hard pulse.[88] Dixon methods are postprocessing approaches that separate water and fat signals, making them available for further analysis.[89]

A tricomponent fitting model was developed to include fat contribution in the acquired MRI signal, using information from the fat nuclear magnetic resonance (NMR) spectrum.[90] Tricomponent fitting has improved estimates of BW and PW fractions in cortical bone and also provided estimates of the fat content in bone. Estimating water fraction by tricomponent T2* fitting improved correlation with µCT-based porosity compared with bicomponent fitting.[90,91] Tricomponent BW and PW biomarkers have also demonstrated higher correlations with the mechanical properties of bone.[91] The tricomponent model avoids BW overestimation in the endosteal side of the cortex, a common miscalculation with bicomponent

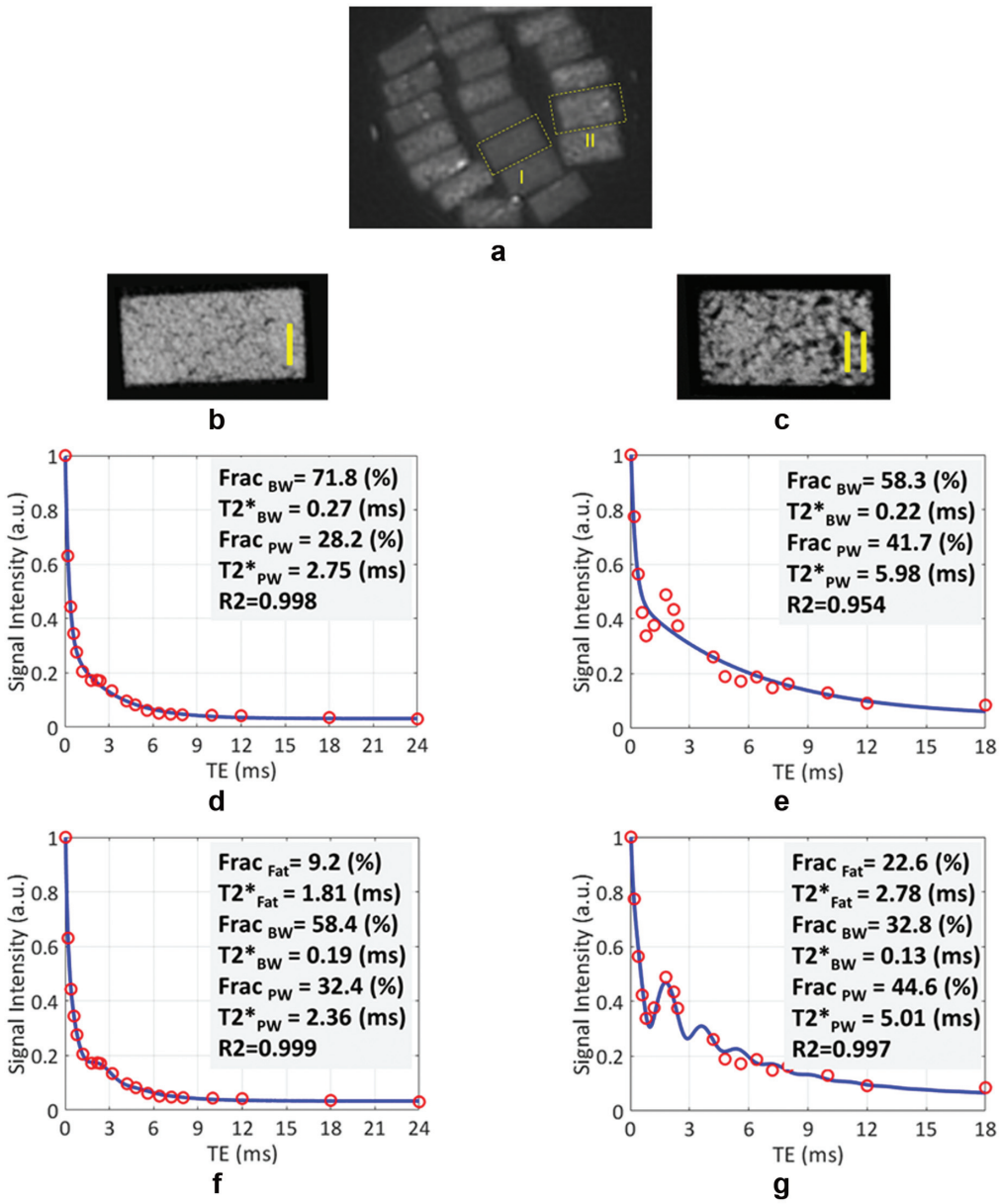

Fig. 7 Ultrashort echo time (UTE) magnetic resonance imaging (MRI) and micro computed tomography (μCT) images of two representative cortical bone strips harvested from different donors possessing different porosities, in addition to bicomponent and tricomponent T2* fitting results. (**a**) UTE MRI (TE = 0.032 ms) image of a set of cortical bone strips with ~ 4 × 2-mm cross sections soaked in Fomblin that produces no signal with MRI. (**b, c**) The μCT images of representative cortical bone strips from a 47-year-old man and a 57-year-old woman, respectively. (**d, e**) Bicomponent T2* fittings for the bone strips are shown in (b) and (c), respectively. (**f, g**) Tricomponent T2* fittings for bone strips are shown in (a) and (b), respectively. The oscillating signal decay in cortical bone specimens is better fitted by including the signal contribution of fat using the tricomponent model (higher fitting R_2 values). a.u., arbitrary unit. This figure was previously presented by Jerban et al.[91] Reprinting permission is granted through the RightsLink system. The figure is modified for presentation purposes.

analysis.[90,91] Nevertheless, the estimated fat content using a tricomponent fitting model needs to be validated in future investigations.

►**Fig. 7a** shows a UTE MRI image of a set of cortical bone strips with 4 × 2-mm cross sections placed in a 1-inch birdcage coil.[91] ►**Fig. 7b, c** illustrates the μCT images of samples I and II with 15% and 33% average porosities, respectively.[91] Bicomponent and tricomponent fitting analyses are shown in ►**Fig. 7d–g** for both specimens. Sample II possesses a higher porosity and shows a significant oscillating signal, which is well fitted using the tricomponent model.

Organic Matrix Biomarkers Using Ultrashort Echo Time Magnetization Transfer

Bone organic matrix biomarkers can provide additional information about bone remodeling status and mechanical properties. Direct quantification of protons in collagen and other organic molecules is challenging with the current MRI hardware because such protons possess extremely short T2*s.[92] Magnetization transfer (MT) imaging combined with UTE MRI was proposed to indirectly detect protons in the organic matrix.[93,94] With MT techniques, a high-power saturation RF

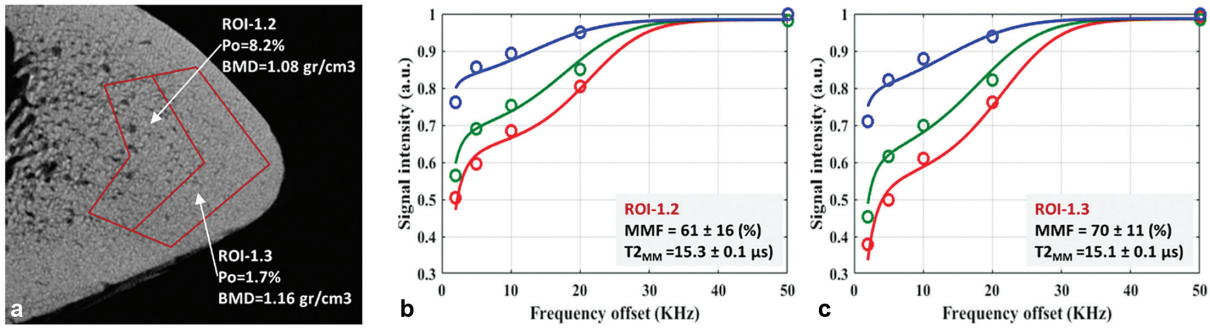

Fig. 8 (**a**) Micro computed tomography (µCT) image of a representative tibial specimen (male, 73-year-old) focused on the anterior tibia with two selected regions of interest (ROIs) in the middle and outer layers. The measured porosity (Po) in the middle layer (ROI-1.2) is higher than that of the outer layer (ROI-1.3). The two-pool magnetization transfer (MT) model analyses in (**b**) ROI-1.2 and (**c**) ROI-1.3 used three pulse saturation powers (500 degrees in blue, 1,000 degrees in green, and 1,500 degrees in red) and five frequency offsets (2, 5, 10, 20, and 50 kHz). MMF and T2MM refer to macromolecular fraction and macromolecular T2, respectively. a.u., arbitrary unit; BMD, bone mineral density. This figure was previously presented by Jerban et al.[94] Reprinting permission is granted through the RightsLink system. The figure is modified for presentation purposes.

pulse is applied with a frequency offset from the water resonance frequency to saturate the magnetization of protons in the organic matrix. Saturated magnetization is transferred from the organic matrix to neighboring BW and PW protons that can be imaged with UTE MRI. UTE-MT assessment of the organic matrix protons, such as the MT ratio, significantly correlates with bone microstructural and mechanical properties.[95]

The magnitude of the transferred saturation is a function of the macromolecular proton fraction (MMF), macromolecular proton transverse relaxation time (T2MM), and exchange rates between pools. These parameters can be estimated with a two-pool model using UTE-MT data acquired with a series of RF pulse power levels and frequency offsets.[93] MMF derived from UTE-MT modeling showed a strong correlation with cortical bone microstructure measured via µCT and histomorphometry[83,94] and with cortical bone mechanical properties.[64,82,83,94]

►**Fig. 8** demonstrates differences in UTE-MT modeling results for a dense and a porous region of a representative tibial bone specimen.[94] Two-pool MT modeling was performed using three MT saturation pulse powers (500, 1,000, and 1,500 degrees) and five off-resonance frequencies (2, 5, 10, 20, and 50 kHz). Higher MMF and lower T2MM values were measured for the denser bone region, with lower µCT-based porosity yet higher vBMD.

Macromolecular proton density (MMPD) can be calculated as a function of MMF and TWPD.[64] MMPD can demonstrate organic matrix density independent of the water content density. ►**Fig. 9** shows in vivo MMF and MMPD maps in the tibial midshaft of a representative OPo patient compared with a normal subject. MMF and MMPD are lower in the OPo patient.

Mineral Content Biomarkers

Although radiograph-based methods (DEXA and CT) are the gold standards for bone mineral assessment, UTE MRI has shown the potential to assess surrogate measures of BMD. An accurate surrogate measure of BMD in combination with the water and organic matrix biomarkers can complete the quantitative MRI biomarker panel in bone evaluation. Such a single-modality imaging of bone can provide information about all major bone components and potentially facilitate clinical decision-making.

Quantitative Susceptibility Mapping Biomarker

Magnetic susceptibility of bone can be mapped using the phase changes in the MRI signal. Bone regions with stronger magnetic susceptibilities undergo faster evolution of phase than regions with lower susceptibility. Dimov et al[96] developed a quantitative susceptibility mapping (QSM) technique

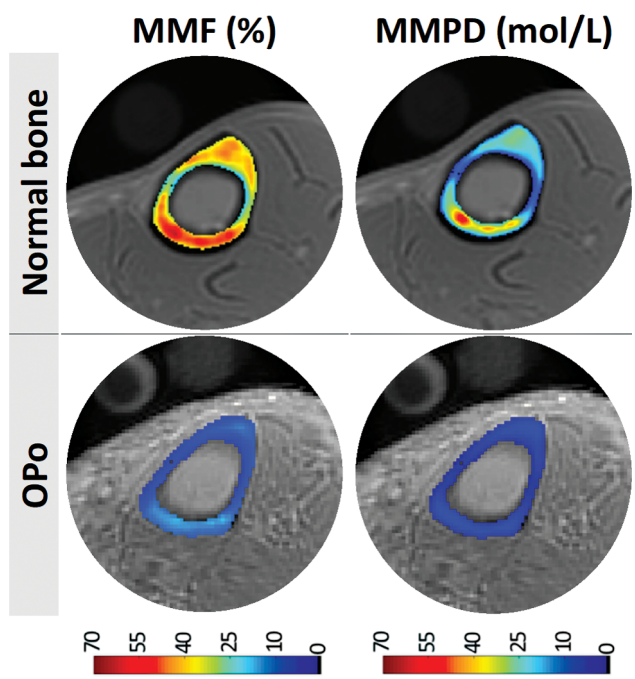

Fig. 9 Generated macromolecular proton fraction (MMF) and macromolecular proton-density (MMPD) maps for (first row) a representative subject with normal bone (a 35-year-old woman) and (second row) a representative patient with osteoporosis (OPo) (a 76-year-old woman). For these examples, MMF and MMPD are higher in the patient with OPo.

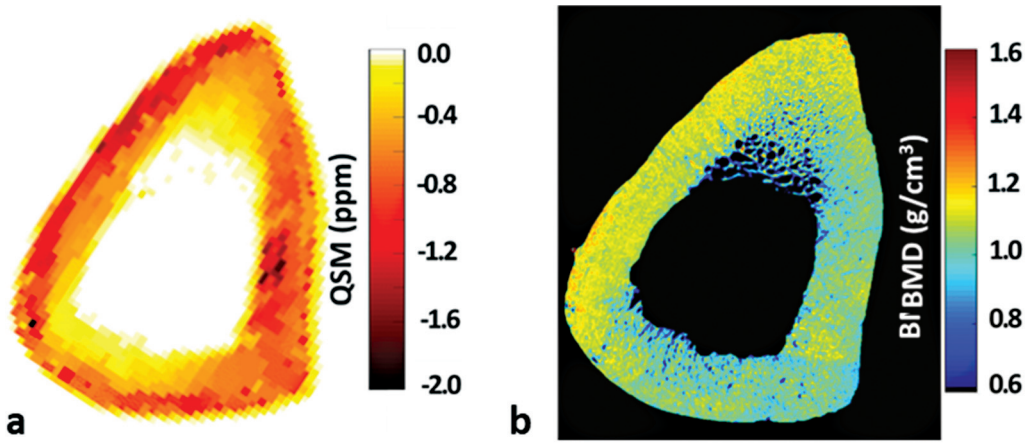

Fig. 10 (**a**) Quantitative susceptibility map (QSM) using Cones three-dimensional (3D) ultrashort echo time (UTE) magnetic resonance imaging (MRI) scans (0.5 × 0.5 × 2-mm voxel size) of a representative tibial midshaft cortical bone sample (45-year-old woman). (**b**) A micro computed tomography (μCT)-based volumetric bone mineral density (vBMD) map of the same specimen. Local maxima in the QSM map correspond to the regions of high vBMD in μCT-based maps. This figure was previously presented by Jerban et al.[97] Reprinting permission is granted through the RightsLink system. The figure is modified for presentation purposes.

combined with UTE acquisition (UTE-QSM) to detect mineral variations in the porcine hoof and human distal femur. They reported significant correlations between radial UTE-QSM values and radiograph attenuation in Hounsfield units measured with CT. UTE-QSM was later investigated in human tibial cortical bone specimens, and a significant correlation with vBMD was observed.[97] ►**Fig. 10** illustrates the UTE-QSM and vBMD (μCT) map in a representative tibial bone specimen. Local maxima of the QSM map qualitatively correspond to the regions of high vBMD in μCT-based maps.[97]

Ultrashort Echo Time ^{31}P Proton Density

Phosphorus (i.e., ^{31}P) imaging acquired with UTE, WASPI, or ZTE MR sequences was used for bone mineral estimation in several studies.[58,62,98] Animal model studies have demonstrated a high sensitivity of phosphorus imaging in detecting compromised BMD in hypophosphatemia-induced osteomalacia at 9.4 T.[99–101] The feasibility of in vivo phosphorus imaging in human subjects was reported at 1.5 T using UTE-based imaging of the tibia and femoral head.[44] More recent bone phosphorus imaging studies at 3 T used ZTE acquisitions and observed a significant reduction of phosphorus density (i.e., BMD) associated with OPo in postmenopausal female subjects.[58,102] Phosphorus imaging can be considered a direct method of mineral imaging compared with the previously discussed QSM method that evaluates mineral density based on its magnetic susceptibility. However, the hardware adjustment necessary for phosphorus imaging has resulted in the underutilization of this technique in bone assessment, even in research centers.

Other Biomarkers in Trabecular Bone

Several MRI-based analyses of trabecular bone have been reported using marrow relaxometry or magnetic susceptibility measurements.[47,49,103–105] These techniques can provide indirect quantifications of trabecular bone density and structure while using low-resolution MRI images.[103,104,106,107] The strong susceptibility between trabeculae and marrow interface leads to greatly reduced relaxation times for bone marrow. The reduction of bone marrow relaxation time in the presence of bone trabeculae depends on many factors, including bone volume and bone-specific surface.[47,49] Bone marrow relaxation times were shown to be correlated with BMD in different studies.[47–49,106–108] Moreover, trabeculae possess stronger magnetic susceptibility compared with bone marrow. Thus the trabecular bone sites with stronger magnetic susceptibilities correspond to regions with higher average BMD. Strong correlations between QSM and BMD in the trabecular bone of the spine and ankle were reported in previous studies using clinical MRI sequences.[105,109]

Alternatively, several research groups have focused on bone marrow composition analysis, providing fat and water proton fractions through MR spectroscopy[110–115] or iterative decomposition of water and fat with echo asymmetry and least-squares estimation (IDEAL).[116–119] Several studies reported that FF in marrow negatively correlated with BMD and bone volume fraction in trabecular bone.[110–117]

Conclusions

Standard imaging-based bone biomarkers cannot rigorously characterize the organic matrix, water, and fat that together represent at least 50% of the bone volume. MRI-based biomarkers, championed by UTE MRI acquisition, can characterize all major compartments of the bone. Such single-modality imaging of bone potentially provides a new tool to better understand bone disease mechanisms and evaluate clinical intervention strategies. Combined basic UTE and IR-UTE sequences can quantify TW, BW, and PW. UTE tricomponent T2* analysis distinguishes between BW and PW signals and fractions in addition to providing FF assessment. UTE-MT sequences can quantify the organic matrix in bone, and UTE-QSM sequences provide a surrogate assessment of BMD. Rapid UTE-based techniques (e.g., 5-minute scan time) to measure water components can move to clinical studies

with limited optimizations. MRI-based organic and mineral matrix biomarkers require more optimization and acceleration via parallel imaging, compressed sensing, or artificial intelligence techniques to achieve an acceptable scanning time appropriate for clinical studies.

Source of Funding
The authors acknowledge grant support from the National Institutes of Health (K01AR080257, R01AR068987, R01AR062581, R01AR075825, R01AR078877, and 5P30AR073761) and Veterans Affairs Clinical Science and Rehabilitation R&D (I01CX001388, I01BX005952, and I01CX000625).

Conflict of Interest
None declared.

References

1 Clarke B. Normal bone anatomy and physiology. Clin J Am Soc Nephrol 2008;3(Suppl 3):S131–S139
2 Cowin SC. Bone poroelasticity. J Biomech 1999;32(03):217–238
3 Ritchie RO, Buehler MJ, Hansma P. Plasticity and toughness in bone. Phys Today 2009;62(06):41–47
4 Ott SM. Cortical or trabecular bone: what's the difference? Am J Nephrol 2018;47(06):373–375
5 Macdonald HM, Nishiyama KK, Kang J, Hanley DA, Boyd SK. Age-related patterns of trabecular and cortical bone loss differ between sexes and skeletal sites: a population-based HR-pQCT study. J Bone Miner Res 2011;26(01):50–62
6 Wang X, Ni Q. Determination of cortical bone porosity and pore size distribution using a low field pulsed NMR approach. J Orthop Res 2003;21(02):312–319
7 Nyman JS, Ni Q, Nicolella DP, Wang X. Measurements of mobile and bound water by nuclear magnetic resonance correlate with mechanical properties of bone. Bone 2008;42(01):193–199
8 Horch RA, Nyman JS, Gochberg DF, Dortch RD, Does MD. Characterization of 1H NMR signal in human cortical bone for magnetic resonance imaging. Magn Reson Med 2010;64(03): 680–687
9 Diaz E, Chung CB, Bae WC, et al. Ultrashort echo time spectroscopic imaging (UTESI): an efficient method for quantifying bound and free water. NMR Biomed 2012;25(01):161–168
10 Biswas R, Bae W, Diaz E, et al. Ultrashort echo time (UTE) imaging with bi-component analysis: bound and free water evaluation of bovine cortical bone subject to sequential drying. Bone 2012;50 (03):749–755
11 Ong HH, Wright AC, Wehrli FW. Deuterium nuclear magnetic resonance unambiguously quantifies pore and collagen-bound water in cortical bone. J Bone Miner Res 2012;27(12):2573–2581
12 Du J, Bydder GM. Qualitative and quantitative ultrashort-TE MRI of cortical bone. NMR Biomed 2013;26(05):489–506
13 Teitelbaum SL. Bone resorption by osteoclasts. Science 2000;289 (5484):1504–1508
14 Wu Y, Humphrey MB, Nakamura MC. Osteoclasts—the innate immune cells of the bone. Autoimmunity 2008;41(03):183–194
15 Cabral HWS, Andolphi BFG, Ferreira BVC, et al. The use of biomarkers in clinical osteoporosis. Rev Assoc Med Bras 2016; 62(04):368–376
16 Kuo TR, Chen CH. Bone biomarker for the clinical assessment of osteoporosis: recent developments and future perspectives. Biomark Res 2017;5(01):18
17 Shetty S, Kapoor N, Bondu JD, Thomas N, Paul TV. Bone turnover markers: emerging tool in the management of osteoporosis. Indian J Endocrinol Metab 2016;20(06):846–852
18 Vasikaran S, Eastell R, Bruyère O, et al; IOF-IFCC Bone Marker Standards Working Group. Markers of bone turnover for the prediction of fracture risk and monitoring of osteoporosis treatment: a need for international reference standards. Osteoporos Int 2011;22(02):391–420
19 Edwards MH, Dennison EM, Aihie Sayer A, Fielding R, Cooper C. Osteoporosis and sarcopenia in older age. Bone 2015;80:126–130
20 Kaplan SJ, Pham TN, Arbabi S, et al. Association of radiologic indicators of frailty with 1-year mortality in older trauma patients: opportunistic screening for sarcopenia and osteopenia. JAMA Surg 2017;152(02):e164604
21 Zioupos P, Currey JD, Hamer AJ. The role of collagen in the declining mechanical properties of aging human cortical bone. J Biomed Mater Res 1999;45(02):108–116
22 Wang X, Shen X, Li X, Agrawal CM. Age-related changes in the collagen network and toughness of bone. Bone 2002;31(01): 1–7
23 Nyman JS, Roy A, Shen X, Acuna RL, Tyler JH, Wang X. The influence of water removal on the strength and toughness of cortical bone. J Biomech 2006;39(05):931–938
24 Wehrli FW, Fernández-Seara MA. Nuclear magnetic resonance studies of bone water. Ann Biomed Eng 2005;33(01):79–86
25 Baffour FI, Glazebrook KN, Ferrero A, et al. Photon-counting detector CT for musculoskeletal imaging: a clinical perspective. AJR Am J Roentgenol 2023;220(04):551–560
26 Laugier P. Instrumentation for in vivo ultrasonic characterization of bone strength. IEEE Trans Ultrason Ferroelectr Freq Control 2008;55(06):1179–1196
27 Raum K, Grimal Q, Varga P, Barkmann R, Glüer CC, Laugier P. Ultrasound to assess bone quality. Curr Osteoporos Rep 2014;12 (02):154–162
28 Jenson F, Padilla F, Bousson V, Bergot C, Laredo JD, Laugier P. In vitro ultrasonic characterization of human cancellous femoral bone using transmission and backscatter measurements: relationships to bone mineral density. J Acoust Soc Am 2006;119 (01):654–663
29 Karjalainen JP, Riekkinen O, Kröger H. Pulse-echo ultrasound method for detection of post-menopausal women with osteoporotic BMD. Osteoporos Int 2018;29(05):1193–1199
30 Grimal Q, Laugier P. Quantitative ultrasound assessment of cortical bone properties beyond bone mineral density. IRBM 2019;40(01):16–24
31 Chin KY, Ima-Nirwana S. Calcaneal quantitative ultrasound as a determinant of bone health status: what properties of bone does it reflect? Int J Med Sci 2013;10(12):1778–1783
32 Han S, Rho J, Medige J, Ziv I, Medige J. Ultrasound velocity and broadband attenuation over a wide range of bone mineral density. Osteoporos Int 1996;6(04):291–296
33 Lasschuit JWJ, Center JR, Greenfield JR, Tonks KTT. Comparison of calcaneal quantitative ultrasound and bone densitometry parameters as fracture risk predictors in type 2 diabetes mellitus. Diabet Med 2020;37(11):1902–1909
34 Yen CC, Lin WC, Wang TH, et al. Pre-screening for osteoporosis with calcaneus quantitative ultrasound and dual-energy X-ray absorptiometry bone density. Sci Rep 2021;11(01):15709
35 Schraders K, Zatta G, Kruger M, et al. Quantitative ultrasound and dual X-ray absorptiometry as indicators of bone mineral density in young women and nutritional factors affecting it. Nutrients 2019;11(10):2336
36 Casciaro S, Conversano F, Pisani P, Muratore M. New perspectives in echographic diagnosis of osteoporosis on hip and spine. Clin Cases Miner Bone Metab 2015;12(02):142–150
37 McCloskey EV, Kanis JA, Odén A, et al. Predictive ability of heel quantitative ultrasound for incident fractures: an individual-level meta-analysis. Osteoporos Int 2015;26(07):1979–1987
38 Yang L, Udall WJM, McCloskey EV, Eastell R. Distribution of bone density and cortical thickness in the proximal femur and their association with hip fracture in postmenopausal women: a

quantitative computed tomography study. Osteoporos Int 2014; 25(01):251–263
39 Ma YJ, Jerban S, Jang H, Chang D, Chang EY, Du J. Quantitative ultrashort echo time (UTE) magnetic resonance imaging of bone: an update. Front Endocrinol (Lausanne) 2020;11(01):567417
40 Jerban S, Chang DG, Ma Y, Jang H, Chang EY, Du J. An update in qualitative imaging of bone using ultrashort echo time magnetic resonance. Front Endocrinol (Lausanne) 2020;11(01):555756
41 Jerban S, Ma Y, Wei Z, Jang H, Chang EY, Du J. Quantitative magnetic resonance imaging of cortical and trabecular bone. Semin Musculoskelet Radiol 2020;24(04):386–401
42 Ma Y, Jang H, Jerban S, et al. Making the invisible visible-ultrashort echo time magnetic resonance imaging: technical developments and applications. Appl Phys Rev 2022;9(04):041303
43 Reichert ILH, Robson MD, Gatehouse PD, et al. Magnetic resonance imaging of cortical bone with ultrashort TE pulse sequences. Magn Reson Imaging 2005;23(05):611–618
44 Robson MD, Gatehouse PD, Bydder GM, Neubauer S. Human imaging of phosphorus in cortical and trabecular bone in vivo. Magn Reson Med 2004;51(05):888–892
45 Chang EY, Du J, Chung CB. UTE imaging in the musculoskeletal system. J Magn Reson Imaging 2015;41(04):870–883
46 Manhard MK, Nyman JS, Does MD. Advances in imaging approaches to fracture risk evaluation. Transl Res 2017; 181:1–14
47 Wehrli FW. Magnetic resonance of calcified tissues. J Magn Reson 2013;229:35–48
48 Wehrli FW, Song HK, Saha PK, Wright AC. Quantitative MRI for the assessment of bone structure and function. NMR Biomed 2006;19(07):731–764
49 Majumdar S. Magnetic resonance imaging of trabecular bone structure. Top Magn Reson Imaging 2002;13(05):323–334
50 Sharma AK, Toussaint ND, Elder GJ, et al. Magnetic resonance imaging based assessment of bone microstructure as a non-invasive alternative to histomorphometry in patients with chronic kidney disease. Bone 2018;114(114):14–21
51 Chang G, Deniz CM, Honig S, et al. Feasibility of three-dimensional MRI of proximal femur microarchitecture at 3 Tesla using 26 receive elements without and with parallel imaging. J Magn Reson Imaging 2014;40(01):229–238
52 Han M, Chiba K, Banerjee S, Carballido-Gamio J, Krug R. Variable flip angle three-dimensional fast spin-echo sequence combined with outer volume suppression for imaging trabecular bone structure of the proximal femur. J Magn Reson Imaging 2015; 41(05):1300–1310
53 Wehrli FW. Structural and functional assessment of trabecular and cortical bone by micro magnetic resonance imaging. J Magn Reson Imaging 2007;25(02):390–409
54 Du J, Hermida JC, Diaz E, et al. Assessment of cortical bone with clinical and ultrashort echo time sequences. Magn Reson Med 2013;70(03):697–704
55 Bae WC, Patil S, Biswas R, et al. Magnetic resonance imaging assessed cortical porosity is highly correlated with μCT porosity. Bone 2014;66:56–61
56 Bydder M, Carl M, Bydder GM, Du J. MRI chemical shift artifact produced by center-out radial sampling of k-space: a potential pitfall in clinical diagnosis. Quant Imaging Med Surg 2021;11 (08):3677–3683
57 Manhard MK, Horch RA, Gochberg DF, Nyman JS, Does MD. In vivo quantitative MR imaging of bound and pore water in cortical bone. Radiology 2015;277(01):221–229
58 Zhao X, Song HK, Seifert AC, Li C, Wehrli FW. Feasibility of assessing bone matrix and mineral properties in vivo by combined solid-state 1H and 31P MRI. PLoS One 2017;12(03): e0173995
59 Du J, Carl M, Bydder M, Takahashi A, Chung CB, Bydder GM. Qualitative and quantitative ultrashort echo time (UTE) imaging of cortical bone. J Magn Reson 2010;207(02):304–311
60 Li C, Seifert AC, Rad HS, et al. Cortical bone water concentration: dependence of MR imaging measures on age and pore volume fraction. Radiology 2014;272(03):796–806
61 Rad HS, Lam SCB, Magland JF, et al. Quantifying cortical bone water in vivo by three-dimensional ultra-short echo-time MRI. NMR Biomed 2011;24(07):855–864
62 Seifert AC, Wehrli FW. Solid-state quantitative (1)H and (31)P MRI of cortical bone in humans. Curr Osteoporos Rep 2016;14 (03):77–86
63 Techawiboonwong A, Song HK, Leonard MB, Wehrli FW. Cortical bone water: in vivo quantification with ultrashort echo-time MR imaging. Radiology 2008;248(03):824–833
64 Jerban S, Ma Y, Li L, et al. Volumetric mapping of bound and pore water as well as collagen protons in cortical bone using 3D ultrashort echo time cones MR imaging techniques. Bone 2019; 127(Oct):120–128
65 Jerban S, Ma Y, Jang H, et al. Water proton density in human cortical bone obtained from ultrashort echo time (UTE) MRI predicts bone microstructural properties. Magn Reson Imaging 2020;67(01):85–89
66 Jones BC, Wehrli FW, Kamona N, et al. Automated, calibration-free quantification of cortical bone porosity and geometry in postmenopausal osteoporosis from ultrashort echo time MRI and deep learning. Bone 2023;171:116743
67 Ma YJ, Lu X, Carl M, et al. Accurate T_1 mapping of short T_2 tissues using a three-dimensional ultrashort echo time cones actual flip angle imaging-variable repetition time (3D UTE-Cones AFI-VTR) method. Magn Reson Med 2018;80(02):598–608
68 Du J, Takahashi AM, Bae WC, Chung CB, Bydder GM. Dual inversion recovery, ultrashort echo time (DIR UTE) imaging: creating high contrast for short-T(2) species. Magn Reson Med 2010;63(02):447–455
69 Horch RA, Gochberg DF, Nyman JS, Does MD. Clinically compatible MRI strategies for discriminating bound and pore water in cortical bone. Magn Reson Med 2012;68(06):1774–1784
70 Lombardi AF, Ma YJ, Jang H, et al. Synthetic CT in musculoskeletal disorders: a systematic review. Invest Radiol 2023;58(01):43–59
71 Du J, Chiang AJT, Chung CB, et al. Orientational analysis of the Achilles tendon and enthesis using an ultrashort echo time spectroscopic imaging sequence. Magn Reson Imaging 2010;28 (02):178–184
72 Manhard MK, Uppuganti S, Granke M, Gochberg DF, Nyman JS, Does MD. MRI-derived bound and pore water concentrations as predictors of fracture resistance. Bone 2016;87:1–10
73 Chen J, Grogan SP, Shao H, et al. Evaluation of bound and pore water in cortical bone using ultrashort-TE MRI. NMR Biomed 2015;28(12):1754–1762
74 Abbasi-Rad S, Saligheh Rad H. Quantification of human cortical bone bound and free water in vivo with ultrashort echo time MR imaging: a model-based approach. Radiology 2017;283(03): 862–872
75 Wurnig MC, Calcagni M, Kenkel D, et al. Characterization of trabecular bone density with ultra-short echo-time MRI at 1.5, 3.0 and 7.0 T—comparison with micro-computed tomography. NMR Biomed 2014;27(10):1159–1166
76 Ma YJ, Chen Y, Li L, et al. Trabecular bone imaging using a 3D adiabatic inversion recovery prepared ultrashort TE Cones sequence at 3T. Magn Reson Med 2020;83(05):1640–1651
77 Jerban S, Ma Y, Moazamian D, et al. MRI-based porosity index (PI) and suppression ratio (SR) in the tibial cortex show significant differences between normal, osteopenic, and osteoporotic female subjects. Front Endocrinol (Lausanne) 2023;14:1148345
78 Jerban S, Ma Y, Alenezi S, et al. Ultrashort echo time (UTE) MRI porosity index (PI) and suppression ratio (SR) correlate with the cortical bone microstructural and mechanical properties: ex vivo study. Bone 2023;169:116676
79 Rajapakse CS, Bashoor-Zadeh M, Li C, Sun W, Wright AC, Wehrli FW. Volumetric cortical bone porosity assessment with MR

imaging: validation and clinical feasibility. Radiology 2015;276 (02):526–535
80 Hong AL, Ispiryan M, Padalkar MV, et al. MRI-derived bone porosity index correlates to bone composition and mechanical stiffness. Bone Rep 2019;11(February):100213
81 Bae WC, Chen PC, Chung CB, Masuda K, D'Lima D, Du J. Quantitative ultrashort echo time (UTE) MRI of human cortical bone: correlation with porosity and biomechanical properties. J Bone Miner Res 2012;27(04):848–857
82 Jerban S, Ma Y, Dorthe EW, et al. Assessing cortical bone mechanical properties using collagen proton fraction from ultrashort echo time magnetization transfer (UTE-MT) MRI modeling. Bone Rep 2019;11(02):100220
83 Jerban S, Ma Y, Wong JH, et al. Ultrashort echo time magnetic resonance imaging (UTE-MRI) of cortical bone correlates well with histomorphometric assessment of bone microstructure. Bone 2019;123(123):8–17
84 Seifert AC, Wehrli SL, Wehrli FW. Bi-component T2 * analysis of bound and pore bone water fractions fails at high field strengths. NMR Biomed 2015;28(07):861–872
85 Du J, Bydder M, Takahashi AM, Chung CB. Two-dimensional ultrashort echo time imaging using a spiral trajectory. Magn Reson Imaging 2008;26(03):304–312
86 Nazaran A, Carl M, Ma Y, et al. Three-dimensional adiabatic inversion recovery prepared ultrashort echo time cones (3D IR-UTE-Cones) imaging of cortical bone in the hip. Magn Reson Imaging 2017;44(Dec):60–64
87 Li S, Ma L, Chang EY, et al. Effects of inversion time on inversion recovery prepared ultrashort echo time (IR-UTE) imaging of bound and pore water in cortical bone. NMR Biomed 2015;28 (01):70–78
88 Ma YJ, Jerban S, Jang H, Chang EY, Du J. Fat suppression for ultrashort echo time imaging using a novel soft-hard composite radiofrequency pulse. Magn Reson Med 2019;82(06):2178–2187
89 Jang H, Carl M, Ma Y, et al. Fat suppression for ultrashort echo time imaging using a single-point Dixon method. NMR Biomed 2019;32(05):e4069
90 Lu X, Jerban S, Wan L, et al. Three-dimensional ultrashort echo time imaging with tricomponent analysis for human cortical bone. Magn Reson Med 2019;82(01):348–355
91 Jerban S, Lu X, Dorthe EW, et al. Correlations of cortical bone microstructural and mechanical properties with water proton fractions obtained from ultrashort echo time (UTE) MRI tricomponent T2* model. NMR Biomed 2020;33(03):e4233
92 Ma YJ, Chang EY, Bydder GM, Du J. Can ultrashort-TE (UTE) MRI sequences on a 3-T clinical scanner detect signal directly from collagen protons: freeze-dry and D2 O exchange studies of cortical bone and Achilles tendon specimens. NMR Biomed 2016;29(07):912–917
93 Ma YJ, Chang EY, Carl M, Du J. Quantitative magnetization transfer ultrashort echo time imaging using a time-efficient 3D multispoke Cones sequence. Magn Reson Med 2018;79 (02):692–700
94 Jerban S, Ma Y, Wan L, et al. Collagen proton fraction from ultrashort echo time magnetization transfer (UTE-MT) MRI modelling correlates significantly with cortical bone porosity measured with micro-computed tomography (μCT). NMR Biomed 2019;32(02):e4045
95 Chang EY, Bae WC, Shao H, et al. Ultrashort echo time magnetization transfer (UTE-MT) imaging of cortical bone. NMR Biomed 2015;28(07):873–880
96 Dimov AV, Liu Z, Spincemaille P, Prince MR, Du J, Wang Y. Bone quantitative susceptibility mapping using a chemical species-specific R2* signal model with ultrashort and conventional echo data. Magn Reson Med 2018;79(01):121–128
97 Jerban S, Lu X, Jang H, et al. Significant correlations between human cortical bone mineral density and quantitative susceptibility mapping (QSM) obtained with 3D Cones ultrashort echo time magnetic resonance imaging (UTE-MRI). Magn Reson Imaging 2019;62(October):104–110
98 Seifert AC, Li C, Rajapakse CS, et al. Bone mineral (31)P and matrix-bound water densities measured by solid-state (31)P and (1)H MRI. NMR Biomed 2014;27(07):739–748
99 Anumula S, Wehrli SL, Magland J, Wright AC, Wehrli FW. Ultrashort echo-time MRI detects changes in bone mineralization and water content in OVX rat bone in response to alendronate treatment. Bone 2010;46(05):1391–1399
100 Anumula S, Magland J, Wehrli SL, et al. Measurement of phosphorus content in normal and osteomalacic rabbit bone by solid-state 3D radial imaging. Magn Reson Med 2006;56(05):946–952
101 Anumula S, Magland J, Wehrli SL, Ong H, Song HK, Wehrli FW. Multi-modality study of the compositional and mechanical implications of hypomineralization in a rabbit model of osteomalacia. Bone 2008;42(02):405–413
102 Jones BC, Lee H, Cheng CC, et al. MRI quantification of cortical bone porosity, mineralization, and morphologic structure in postmenopausal osteoporosis. Radiology 2023;307(02):e221810
103 Majumdar S, Thomasson D, Shimakawa A, Genant HK. Quantitation of the susceptibility difference between trabecular bone and bone marrow: experimental studies. Magn Reson Med 1991;22 (01):111–127
104 Ford JC, Wehrli FW. In vivo quantitative characterization of trabecular bone by NMR interferometry and localized proton spectroscopy. Magn Reson Med 1991;17(02):543–551
105 Diefenbach MN, Meineke J, Ruschke S, Baum T, Gersing A, Karampinos DC. On the sensitivity of quantitative susceptibility mapping for measuring trabecular bone density. Magn Reson Med 2019;81(03):1739–1754
106 Majumdar S, Genant HK. A review of the recent advances in magnetic resonance imaging in the assessment of osteoporosis. Osteoporos Int 1995;5(02):79–92
107 Beuf O, Newitt DC, Mosekilde L, Majumdar S. Trabecular structure assessment in lumbar vertebrae specimens using quantitative magnetic resonance imaging and relationship with mechanical competence. J Bone Miner Res 2001;16(08):1511–1519
108 Link TM, Majumdar S, Augat P, et al. Proximal femur: assessment for osteoporosis with T2* decay characteristics at MR imaging. Radiology 1998;209(02):531–536
109 Chen Y, Guo Y, Zhang X, Mei Y, Feng Y, Zhang X. Bone susceptibility mapping with MRI is an alternative and reliable biomarker of osteoporosis in postmenopausal women. Eur Radiol 2018;28 (12):5027–5034
110 Griffith JF, Yeung DKW, Antonio GE, et al. Vertebral bone mineral density, marrow perfusion, and fat content in healthy men and men with osteoporosis: dynamic contrast-enhanced MR imaging and MR spectroscopy. Radiology 2005;236(03):945–951
111 Shih TTF, Chang CJ, Hsu CY, Wei SY, Su KC, Chung HW. Correlation of bone marrow lipid water content with bone mineral density on the lumbar spine. Spine 2004;29(24):2844–2850
112 Griffith JF, Yeung DKW, Antonio GE, et al. Vertebral marrow fat content and diffusion and perfusion indexes in women with varying bone density: MR evaluation. Radiology 2006;241(03): 831–838
113 Griffith JF, Yeung DKW, Ma HT, Leung JCS, Kwok TCY, Leung PC. Bone marrow fat content in the elderly: a reversal of sex difference seen in younger subjects. J Magn Reson Imaging 2012;36(01):225–230
114 Li X, Kuo D, Schafer AL, et al. Quantification of vertebral bone marrow fat content using 3 Tesla MR spectroscopy: reproducibility, vertebral variation, and applications in osteoporosis. J Magn Reson Imaging 2011;33(04):974–979
115 Mostoufi-Moab S, Magland J, Isaacoff EJ, et al. Adverse fat depots and marrow adiposity are associated with skeletal deficits and insulin resistance in long-term survivors of pediatric hematopoietic stem cell transplantation. J Bone Miner Res 2015;30(09): 1657–1666

116 Karampinos DC, Melkus G, Baum T, Bauer JS, Rummeny EJ, Krug R. Bone marrow fat quantification in the presence of trabecular bone: initial comparison between water-fat imaging and single-voxel MRS. Magn Reson Med 2014;71(03):1158–1165
117 Gee CS, Nguyen JTK, Marquez CJ, et al. Validation of bone marrow fat quantification in the presence of trabecular bone using MRI. J Magn Reson Imaging 2015;42(02):539–544
118 Reeder SB, Robson PM, Yu H, et al. Quantification of hepatic steatosis with MRI: the effects of accurate fat spectral modeling. J Magn Reson Imaging 2009;29(06):1332–1339
119 Yu H, Shimakawa A, McKenzie CA, Brodsky E, Brittain JH, Reeder SB. Multiecho water-fat separation and simultaneous R2* estimation with multifrequency fat spectrum modeling. Magn Reson Med 2008;60(05):1122–1134
120 Akbari A, Abbasi-Rad S, Rad HS. T1 correlates age: a short-TE MR relaxometry study in vivo on human cortical bone free water at 1.5T. Bone 2016;83:17–22
121 Du J, Bydder M, Takahashi AM, Carl M, Chung CB, Bydder GM. Short T2 contrast with three-dimensional ultrashort echo time imaging. Magn Reson Imaging 2011;29(04):470–482
122 Johnson EM, Vyas U, Ghanouni P, Pauly KB, Pauly JM. Improved cortical bone specificity in UTE MR imaging. Magn Reson Med 2017;77(02):684–695
123 Breighner RE, Endo Y, Konin GP, Gulotta LV, Koff MF, Potter HG. Zero echo time imaging of the shoulder: enhanced osseous detail by using MR imaging. Radiology 2018;286(03):960–966
124 Weiger M, Pruessmann KP. MRI with zero echo time. Encyclopedia of Magnetic Resonance 2012;1(02):311–322
125 Garwood M, Idiyatullin D, Corum CA, et al. Capturing signals from fast-relaxing spins with frequency-swept MRI: SWIFT. Encyclopedia of Magnetic Resonance 2012;1(02):322–332
126 Grodzki DM, Jakob PM, Heismann B. Ultrashort echo time imaging using pointwise encoding time reduction with radial acquisition (PETRA). Magn Reson Med 2012;67(02):510–518
127 Weiger M, Wu M, Wurnig MC, et al. ZTE imaging with long-T2 suppression. NMR Biomed 2015;28(02):247–254
128 Du J, Takahashi AM, Chung CB. Ultrashort TE spectroscopic imaging (UTESI): application to the imaging of short T2 relaxation tissues in the musculoskeletal system. J Magn Reson Imaging 2009;29(02):412–421
129 Nyman JS, Gorochow LE, Adam Horch R, et al. Partial removal of pore and loosely bound water by low-energy drying decreases cortical bone toughness in young and old donors. J Mech Behav Biomed Mater 2013;22:136–145
130 Ma YJ, West J, Nazaran A, et al. Feasibility of using an inversion-recovery ultrashort echo time (UTE) sequence for quantification of glenoid bone loss. Skeletal Radiol 2018;47(07):973–980
131 Du J, Carl M, Bae WC, et al. Dual inversion recovery ultrashort echo time (DIR-UTE) imaging and quantification of the zone of calcified cartilage (ZCC). Osteoarthritis Cartilage 2013;21(01):77–85
132 Garwood M, DelaBarre L. The return of the frequency sweep: designing adiabatic pulses for contemporary NMR. J Magn Reson 2001;153(02):155–177
133 Ma YJ, Zhu Y, Lu X, Carl M, Chang EY, Du J. Short T_2 imaging using a 3D double adiabatic inversion recovery prepared ultrashort echo time cones (3D DIR-UTE-Cones) sequence. Magn Reson Med 2018;79(05):2555–2563
134 Wu Y, Ackerman JL, Chesler DA, Graham L, Wang Y, Glimcher MJ. Density of organic matrix of native mineralized bone measured by water- and fat-suppressed proton projection MRI. Magn Reson Med 2003;50(01):59–68
135 Cao H, Ackerman JL, Hrovat MI, Graham L, Glimcher MJ, Wu Y. Quantitative bone matrix density measurement by water- and fat-suppressed proton projection MRI (WASPI) with polymer calibration phantoms. Magn Reson Med 2008;60(06):1433 1443
136 Cao H, Nazarian A, Ackerman JL, et al. Quantitative (31)P NMR spectroscopy and (1)H MRI measurements of bone mineral and matrix density differentiate metabolic bone diseases in rat models. Bone 2010;46(06):1582–1590
137 Wu Y, Hrovat MI, Ackerman JL, et al. Bone matrix imaged in vivo by water- and fat-suppressed proton projection MRI (WASPI) of animal and human subjects. J Magn Reson Imaging 2010;31(04):954–963
138 Techawiboonwong A, Song HK, Wehrli FW. In vivo MRI of submillisecond T(2) species with two-dimensional and three-dimensional radial sequences and applications to the measurement of cortical bone water. NMR Biomed 2008;21(01):59–70
139 Li S, Chang EY, Bae WC, et al. Ultrashort echo time bi-component analysis of cortical bone–a field dependence study. Magn Reson Med 2014;71(03):1075–1081
140 Jerban S, Szeverenyi N, Ma Y, et al. Ultrashort echo time MRI (UTE-MRI) quantifications of cortical bone varied significantly at body temperature compared with room temperature. Investig Magn Reson Imaging 2019;23(03):202
141 Jerban S, Ma Y, Nazaran A, et al. Detecting stress injury (fatigue fracture) in fibular cortical bone using quantitative ultrashort echo time-magnetization transfer (UTE-MT): An ex vivo study. NMR Biomed 2018;31(11):e3994
142 Techawiboonwong A, Song HK, Magland JF, Saha PK, Wehrli FW. Implications of pulse sequence in structural imaging of trabecular bone. J Magn Reson Imaging 2005;22(05):647–655

